Driving and detecting ferromagnetic resonance in insulators with the spin Hall effect

Joseph Sklenar,[1,2] Wei Zhang,[1] Matthias B. Jungfleisch,[1] Wanjun Jiang,[1] Houchen Chang,[3] John E. Pearson,[1] Mingzhong Wu,[3] John B. Ketterson,[2] and Axel Hoffmann[1]

[1]*Materials Science Division, Argonne National Laboratory, Argonne, Illinois 60439, USA*

[2]*Department of Physics and Astronomy, Northwestern University, Evanston, Illinois 60208, USA*

[3]*Department of Physics, Colorado State University, Fort Collins, Colorado 80523, USA*

(Received 26 February 2015; revised manuscript received 24 August 2015; published 6 November 2015)

We demonstrate the generation and detection of spin-torque ferromagnetic resonance in $Pt/Y_3Fe_5O_{12}$ (YIG) bilayers. A unique attribute of this system is that the spin Hall effect lies at the heart of both the generation and detection processes and no charge current is passing through the insulating magnetic layer. When the YIG undergoes resonance, a dc voltage is detected longitudinally along the Pt that can be described by two components. One is the mixing of the spin Hall magnetoresistance with the microwave current. The other results from spin pumping into the Pt being converted to a dc current through the inverse spin Hall effect. The voltage is measured with applied magnetic field directions that range from in plane to nearly perpendicular. When compared with theory, we find that the real and imaginary parts of the spin mixing conductance have out-of-plane angular dependences.

DOI: 10.1103/PhysRevB.92.174406 PACS number(s): 76.50.+g, 72.25.Pn, 75.76.+j

I. INTRODUCTION

Magnetic insulators such as $Y_3Fe_5O_{12}$ (YIG) with extremely low magnetic damping serve as promising platforms for low power data transmission [1–5]. In YIG/Pt bilayers the groundbreaking discovery of magnetization dynamics generated by spin orbit torques of Pt contacts [6,7] opens up new opportunities for device concepts combining electronic, spintronic, and magnonic approaches. The spin orbit torques in heavy metals arise from the spin Hall effect (SHE) [8,9], which converts a charge current $\mathbf{J}_c$ to a spin current $\mathbf{J}_s$ with a conversion efficiency dictated by a materials specific parameter, i.e., the spin Hall angle Θ_{SH} [10,11]. The resultant spin current can drive spin-torque ferromagnetic resonance (ST-FMR) in bilayer thin films made from metallic ferromagnets and nonmagnetic metals [12,13]. In such experiments, FMR is driven by the simultaneous Oersted field and oscillating transverse spin current (spin torque) transformed by SHE from the alternating charge current. Electrical detection is made possible via the spin-torque diode effect [14], i.e., the rectification of the time dependent bilayer resistance arising from the anisotropic magnetoresistance (AMR) of the ferromagnet [15–17]. However, such a detection scenario is not possible in magnetic insulators due to missing free electrons coupling to magnetic moments and, thus, the absence of AMR.

In this article, we show experimentally that the SHE of a paramagnetic metal can be used for both excitation and detection of ST-FMR for magnetic insulators. We demonstrate magnetization dynamics of a thin YIG layer induced by spin torque from an adjacent Pt layer, as well as subsequent detection of a dc voltage via the spin-torque diode effect generated by the anisotropic spin Hall magnetoresistance (SMR) of the Pt [16,18–21]. It bears mentioning that the anisotropic resistance of metal films on top of ferromagnetic insulators, and interface effects in general [22–24], are a very active topic, and other mechanisms independent of the SHE such as interface proximity effects [25] and interfacial Rashba effects [26,27] are being explored as contributors. In this work, SMR refers to the dependence of the electrical resistance of the metal on the magnetization direction of an adjacent magnetic insulator and is a result of a simultaneous operation of the SHE and its inverse (ISHE) as a nonequilibrium phenomenon. Microscopically, this anisotropic behavior originates from the dependence of the spin accumulations of conduction electrons at the YIG/Pt interface on the static YIG magnetization. For example, if the static magnetization is aligned with the spin current's polarization at the interface, there is a large backflow [16,28] spin current; on the other hand, if the magnetization is orthogonal to the polarization, a spin current is absorbed at the interface, and consequently the interfacial spin accumulation is reduced.

Models of spin transport at the YIG/Pt interface that exclude proximity effects [29] introduce the spin mixing conductance $G^{\uparrow\downarrow}$ to describe both the magnitude and phase of the interface spin current [30]. This concept has been probed in a comprehensive study [31] involving a suite of experiments such as spin pumping [32,33], spin Seebeck detection [34], and SMR measurements [16,18–21]. It has also been shown that the value of $G^{\uparrow\downarrow}$ for a YIG/Pt interface is heavily dependent on sample fabrication and processing [35]. In these works, the spin mixing conductance is typically described as being purely real. However, for YIG/Pt bilayers, it has been theoretically suggested that a nonzero value of $\mathrm{Im}(G^{\uparrow\downarrow})$ should be considered [19,36]. Furthermore, experiments investigating spin Hall magnetoresistance [37] and the anomalous spin Hall effect in Pt have provided evidence for a nonzero $\mathrm{Im}(G^{\uparrow\downarrow})$ at the YIG/Pt interface [38]. In this work, we are demonstrating that purely electrical excitation and detection of ferromagnetic resonance can be achieved. Furthermore, we will present evidence that for ST-FMR experiments where the magnetic field is tipped out of plane (OOP), a nonzero $\mathrm{Im}(G^{\uparrow\downarrow})$ is required and evolves as a function of the OOP angle.

II. EXPERIMENTAL DETAILS

We fabricated YIG(40 nm)/Pt(6 nm) bilayers by *in situ* magnetron sputtering on single crystal gadolinium gallium garnet (GGG, $Gd_3Ga_5O_{12}$) substrates of 500 μm thickness with

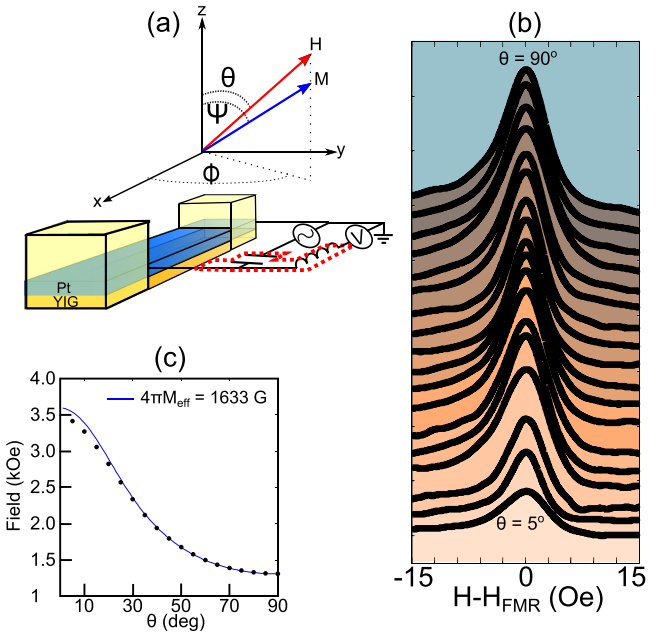

FIG. 1. (Color online) A schematic of the bilayer and ST-FMR setup is shown in (a). In the diagram, **H** indicates an experimentally applied field, and **M** indicates the magnetization vector. θ describes the tipping of **H** from the z axis (thickness direction) and ψ describes the tipping of **M** in the same manner. ϕ is an in-plane angle between the x and y axis; in all our experiments, $\phi = 45^\circ$. (b) ST-FMR traces measured over a range of θ that spans from 90° to 5° in 5° steps. In order to show every resonance, we plot each resonance centered on zero field. (c) shows the θ dependence of the ST-FMR experiments fit to Eq. (4). $4\pi M_{\text{eff}}$ is extracted from this data set to be 1633 G.

[111] orientation under high-purity argon atomsphere [3,39]. The bilayers were subsequently patterned into microstripes in the shape of 500 μm × 100 μm by photolithography and liquid nitrogen cooled ion milling to remove all the YIG/Pt materials except for the bar structure. In a last fabrication step, square contact pads made of Ti/Au (3 nm / 120 nm) are patterned on top of each end of the YIG/Pt stripe via photolithography and lift-off. We configured our setup into a ST-FMR scheme that is illustrated in Fig. 1(a). A bias-tee is utilized to allow for simultaneous transmission of microwaves as well as dc voltage detection across the Pt. We modulate the amplitude of the microwave current at 4 kHz so that the ST-FMR dc signal is detected via a lock-in amplifier to improve signal to noise.

The coordinate system that we will reference throughout this work is shown in Fig. 1(a). The angle ϕ is in-plane and lies between the x and y axis, and it describes the in-plane projection of both the field and magnetization. The polar angle θ describes the applied magnetic field direction OOP, while the polar angle ψ is the calculated OOP component of the magnetization. Due to geometrical demagnetization fields, $\psi > \theta$; for a given θ and applied magnetic field ψ is determined from the following expression,

$$2\pi M_{\text{eff}} \sin 2\psi \csc(\psi - \theta) - H_{\text{ex}} = 0, \tag{1}$$

where M_{eff} is the effective magnetization of the YIG and H_{ex} is the externally applied magnetic field.

III. RESULTS AND DISCUSSION

A. Out-of-plane field dependence

We performed two experiments: The first experiment shown in Fig. 1 (b) fixes ϕ at 45° and varies θ from 90° to 5°. To induce ST-FMR in the YIG we passed a fixed 5.5 GHz signal through the Pt while sweeping H_{ex}. The nominal microwave power level was set to be 10 dBm. When both spin transfer torque (STT) from the SHE and an Oersted drive field is present, the dynamic response of the system is governed by a modified Landau-Lifshitz-Gilbert (LLG) equation of motion [36],

$$\frac{d\hat{\mathbf{M}}}{dt} = -|\gamma|\hat{\mathbf{M}} \times \mathbf{H}_{\text{eff}} + \alpha_\circ \hat{\mathbf{M}} \times \frac{d\hat{\mathbf{M}}}{dt} + \frac{|\gamma|\hbar \mathbf{J}_s}{2eM_s d_F}, \tag{2}$$

where $\mathbf{H}_{\text{eff}}$ includes the Oersted field H_{ac}, demagnetization fields, and the applied external dc field H_{ex}. Additional quantities of importance are the intrinsic damping $\alpha_\circ$ and the spin current at the interface,

$$\mathbf{J}_s = \frac{\text{Re}(G^{\uparrow\downarrow})}{e}\hat{\mathbf{M}} \times (\hat{\mathbf{M}} \times \boldsymbol{\mu}_s) + \frac{\text{Im}(G^{\uparrow\downarrow})}{e}\hat{\mathbf{M}} \times \boldsymbol{\mu}_s + \frac{\hbar}{e}\left(\text{Re}(G^{\uparrow\downarrow})\hat{\mathbf{M}} \times \frac{\partial \hat{\mathbf{M}}}{\partial t} + \text{Im}(G^{\uparrow\downarrow})\frac{\partial \hat{\mathbf{M}}}{\partial t}\right), \tag{3}$$

that originates from the SHE in Pt as well as spin pumping from the ferromagnet. Here, $G^{\uparrow\downarrow}$ is the spin mixing conductance and μ_s is the spin accumulation distribution at the YIG/Pt interface. The oscillatory torque terms that drive the magnetization are the field from the microwave current in H_{eff} and the spin-torque term that includes J_s. The OOP field dependence of the resonances shown in Fig. 1(b) is plotted in Fig. 1(c). In order to extract the effective saturation magnetization of our YIG, we fit [Fig. 1(c)] the out-of-plane angular dependence to the generalized Kittel equation that is given by

$$f = \frac{|\gamma|}{2\pi} 4\pi M_{\text{eff}} \times \sqrt{h^2 + h(\sin\theta \sin\psi - 2\cos\theta\cos\psi) + \cos^2\psi}, \tag{4}$$

where γ is the gyromagnetic ratio taken as 2.8 GHz/kOe, and h is the dimensionless quantity $H/4\pi M_{\text{eff}}$. The extracted effective magnetization is $4\pi M_{\text{eff}} = 1633$ G. We note that this Kittel-like analysis does not account for magnetocrystalline anisotropy or exchange energy. For comparison, in a separate work involving the study of spin waves in other thin YIG films, we measured $4\pi M_{\text{eff}} = 1553$ G [40].

B. In-plane field dependence

The second experiment fixed θ at 90° and varied ϕ from roughly −90° to 270°. For the sake of space we do not show all of the ST-FMR resonance curves. Instead, we show the results in Fig. 2 of fitting the ST-FMR line shape to the superposition of a generic symmetric line shape and antisymmetric line shape,

$$\text{Fit}_{\text{generic}} = \frac{S * \Delta}{\left(H^2 - H_{\text{FMR}}^2\right)^2 + \Delta^2} + \frac{A * \left(H^2 - H_{\text{FMR}}^2\right)}{\left(H^2 - H_{\text{FMR}}^2\right)^2 + \Delta^2}, \tag{5}$$

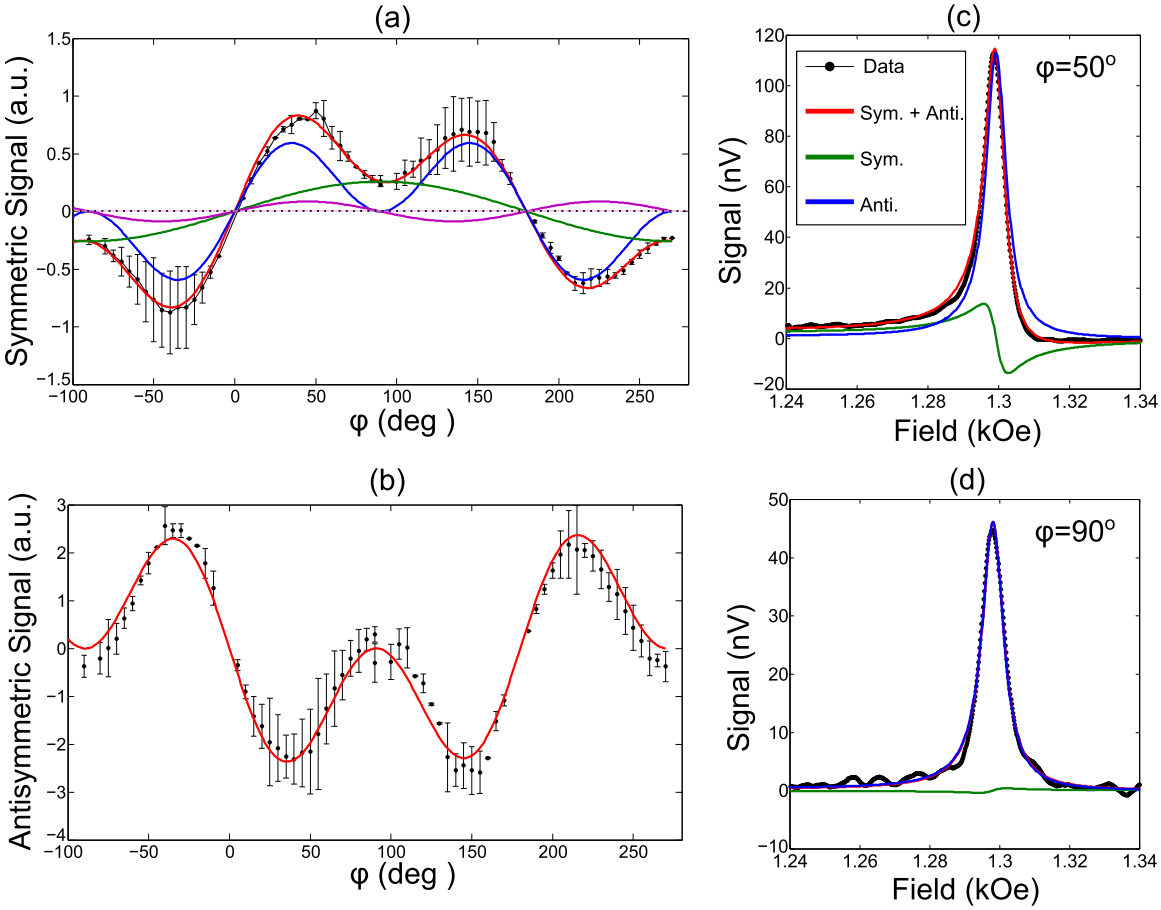

FIG. 2. (Color online) In (a), the symmetric portion of the dc line shape is plotted as a function of the in-plane angle ϕ. The blue curve shown is the $\sin 2\phi \cos\phi$ dependence that comes from the ST-FMR model we use. Not included in the model is a $\sin\phi$ dependence shown in green which may originate from an additional spin pumping term. The purple curve is a $\sin 2\phi$ dependence that may come from inhomogeneous rf fields in our device that are OOP. The sum of all three contributions is plotted in red as a best fit to the data. In (b), we plot the antisymmetric amplitude of the dc line shape and fit it to the expected $\sin 2\phi \cos\phi$ angular dependence. In (c), a representative ST-FMR trace is shown at $\phi = 50^\circ$ where the signal is expected to be nonzero. At $\phi = 50^\circ$ there is clearly both a symmetric and antisymmetric component to the measured line shape. In (d), $\phi = 90^\circ$ and a symmetric signal is observed with a nearly nulled antisymmetric component. At $\phi = 90^\circ$ the model we used to analyze the data predicts that there should be no measurable voltage.

where S is a symmetric amplitude parameter, A is a antisymmetric amplitude parameter, Δ is the square of the linewidth, and H_{FMR} is the field where FMR is occurring, which can be determined from Eq. (4). In Fig. 2(a) the symmetric amplitude parameter is plotted as a function of ϕ, while in Fig. 2(b) the antisymmetric amplitude is plotted as a function of ϕ. Two representative traces of the data are shown at $\phi = 50^\circ$ and $\phi = 90^\circ$ in Figs. 2(c) and 2(d), respectively. The ϕ dependence on the symmetric amplitude was fit to a combination of $\sin 2\phi \cos\phi$, $\sin\phi$, and $\sin 2\phi$ while the antisymmetric amplitude was fit well to $\sin 2\phi \cos\phi$. The implications of the dominant $\sin 2\phi \cos\phi$ and $\sin\phi$ in-plane angular dependences will be discussed. The $\sin 2\phi$ angular dependence is weaker by comparison and is likely due to inhomogeneous rf fields in the device that are out of the plane of the sample [41].

C. Comparison to theory

To explain our experimental observations, we employ a theory developed by Chiba *et al.* [36,42]. Qualitatively, this model describes a dc voltage that develops longitudinally along the Pt film when a microwave charge current flowing through the Pt induces ferromagnetic resonance in the YIG. There are two different contributions to the observed voltage: First, there is an analog to what is observed for Py/Pt bilayers where AMR of the Py mixes with the microwaves to generate a dc voltage at and near the FMR condition [12]. For YIG/Pt the magnetoresistance resides in the Pt and is the SMR [18–20]. Additionally, spin pumping at the YIG/Pt interface can inject a spin current into the Pt that can be converted to a dc charge current via the ISHE.

The theoretical model [36,42] predicts that the voltage generated by spin pumping has a purely symmetric line shape about the resonance condition, and that the voltage induced by SMR can also have a symmetric contribution. Furthermore, the SMR contribution has an antisymmetric contribution to the line shape as well. This model [42] was recently expanded to include a nonzero imaginary part of $G^{\uparrow\downarrow}$, a phase shift parameter δ between the charge current J_c and H_{ac}, and an OOP applied dc Oersted field [36]. δ should be considered to be a property of a given device and, for a fixed excitation

frequency, should be constant. The addition of the nonzero imaginary part of $G^{\uparrow\downarrow}$ along with the phase shift parameter δ allows for additional tunability in the net amplitude of both the antisymmetric as well as the symmetric contribution to the line shape.

According to theory, the line shapes of a ST-FMR experiment for a YIG/Pt bilayer have the following functional forms [36],

$$V_{\mathrm{SMR}} = [S_1 F_S(H_{\mathrm{ex}}) + A_1 F_A(H_{\mathrm{ex}})] \cos\phi \sin 2\phi \sin\psi - [S_2 F_S(H_{\mathrm{ex}}) + A_2 F_A(H_{\mathrm{ex}})] \sin^3\phi \cos\psi \sin 2\psi + A_3 \sin\phi \sin 2\phi \sin 2\psi, \quad (6)$$

$$V_{\mathrm{SP}} = S_3 \cos\phi \sin 2\phi \sin\psi + S_4 \sin^3\phi \cos\psi \sin 2\psi + S_5 \sin\phi \sin 2\phi \sin 2\psi, \quad (7)$$

where V_{SMR} arises from SMR and V_{SP} is from spin pumping. $F_S(H_{\mathrm{ex}})$ is the field dependent symmetric line shape that is given by $\Delta^2/[(H_{\mathrm{ex}} - H_{\mathrm{FMR}})^2 \cos^2(\theta - \psi) + \Delta^2]$. $F_A(H_{\mathrm{ex}})$ is an antisymmetric line shape that is given by $F_S(H_{\mathrm{ex}}) \cos(\theta - \psi)(H_{\mathrm{ex}} - H_{\mathrm{FMR}})/\Delta$. S_1 and S_2 and A_1 through A_3 are coefficients that rely on the mixing of the oscillatory SMR with the charge current, and all end up being proportional to J_c^2; the other relevant parameters, such as Θ_{SH}, $G^{\uparrow\downarrow}$, δ, M_{eff}, d_N, and d_F, are imbedded within these coefficients [36]. Here, d_N is the 6 nm Pt thickness, and d_F is the 40 nm YIG thickness. Two other parameters not yet mentioned are contained within these coefficients; they are the Pt resistivity ρ and the spin diffusion length λ. In our analysis we use $\lambda = 1.2$ nm; this value was determined for Pt by spin pumping experiments in Py/Pt bilayers [43]. S_3 through S_5 are spin pumping coefficients that are similarly proportional to J_c^2 and depend on the same quantities listed above for the SMR terms. Complete expressions for these coefficients can be found elsewhere [36].

In our analysis there are three fitting parameters assumed to be independent of θ and ϕ: Θ_{SH}, J_c, and δ. We did not directly assume that the magnitude or complex composition of $G^{\uparrow\downarrow}$ was independent of θ or ϕ. Because we have previously measured the Θ_{SH} of Pt to be 0.09, we analyze our data with this value in mind [43]. Because the magnitude of $G^{\uparrow\downarrow}$ is free, we found various values of J_c could be used with reasonable $G^{\uparrow\downarrow}$ counterparts. In fact, these two parameters are strongly anticorrelated. However, we found that a given J_c *does not* ensure that the magnitude of $G^{\uparrow\downarrow}$ remains relatively constant over all θ. We typically see an increase in the magnitude of $G^{\uparrow\downarrow}$ as the field is tipped OOP. The value of J_c (9×10^8 A/m^2) chosen here minimized the variation of $G^{\uparrow\downarrow}$ over θ for our initial analysis. In other ST-FMR experiments the parameter δ has been assumed to be zero, therefore we will begin our discussion by following this example [12,13].

With Θ_{SH}, J_c, and δ fixed, one is poised to investigate the magnitude and complex behavior of $G^{\uparrow\downarrow}$ as a function of θ at $\phi = 45°$ based on the data shown in Fig. 1(b). Before doing so, there is one further detail. In Fig. 2(a) the symmetric component of the line shape does not go to zero at $\phi = 90°$, as seen explicitly in Fig. 2(d). The model we employ from Chiba predicts *only* a $\sin 2\phi \cos\phi$ in-plane ϕ dependence; the question of what to make of the additional $\sin\phi$ term and how to proceed in an analysis with the model arises. In terms of how to proceed with the analysis, we tried two methods. The first method is to be agnostic of the additional ϕ dependence when treating the θ dependence. This essentially means the data are taken as is, and the model is applied. The second method attempts to correct the data by assuming that the $\sin\phi$ contribution to the symmetric signal is excessive and should be subtracted out. At $\theta = 90°$ the $\sin\phi$ contribution is roughly 30% of the total symmetric amplitude. We then assume that this additional $\sin\phi$ term has an OOP angular dependence given as $\sin\phi \sin\psi$. This choice is justifiable for the following reasons. A possible origin for this $\sin\phi \sin\psi$ symmetric signal is incoherent spin pumping from additional heating when the sample is at FMR; this would then be a spin Seebeck signal in origin [34]. This additional spin pumping would be expected to have a $\sin\phi \sin\psi$ OOP dependence. A $\sin\phi \sin\psi$ dependence is also the simplest OOP dependence that guarantees that a signal would be observed at $\theta = 90°$.

1. Analysis without correction for possible spin Seebeck contribution

We now present the results from our approach of not assuming any corrections are needed to the symmetric line shape. Figure 3(a) shows the θ dependence for the magnitude of $G^{\uparrow\downarrow}$ for the typical assumption of $\delta = 0°$ as black circles. The complex behavior of $G^{\uparrow\downarrow}$ is plotted in Fig. 3(b), where the $\mathrm{Re}(G^{\uparrow\downarrow})$ is indicated as black circles and the $\mathrm{Im}(G^{\uparrow\downarrow})$ is shown as orange squares. Here, one sees that the composition of $G^{\uparrow\downarrow}$ is purely imaginary from $\theta = 35°$ to 90°. This region is indicated as **II** in the plot. For small values of θ (<35°) the

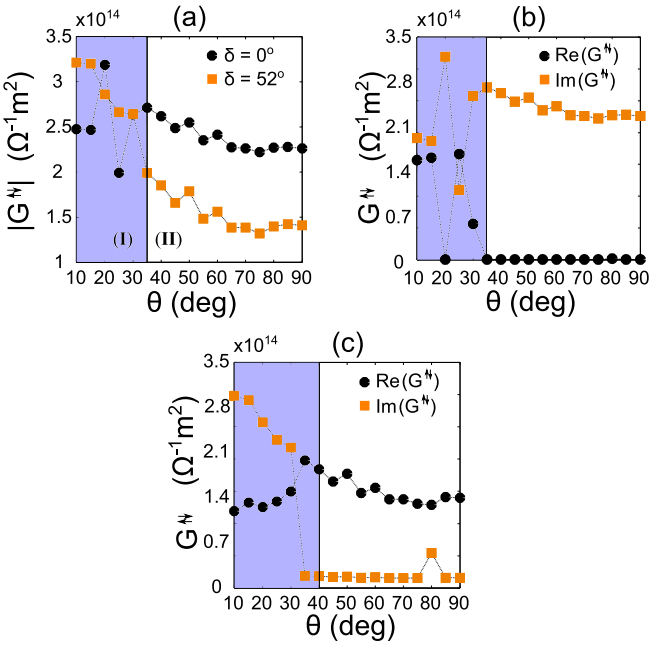

FIG. 3. (Color online) The results of the θ dependence on both the real and imaginary components of the spin mixing conductance are shown above. In (a), $|G^{\uparrow\downarrow}|$ is plotted as a function of θ for two different assumed values of δ. The circles represent $\delta = 0°$ and the squares represent $\delta = 52°$. In (b), the real and imaginary components of $G^{\uparrow\downarrow}$ are plotted as a function of θ for $\delta = 0°$. In (c), the real and imaginary components are plotted for $\delta = -52°$.

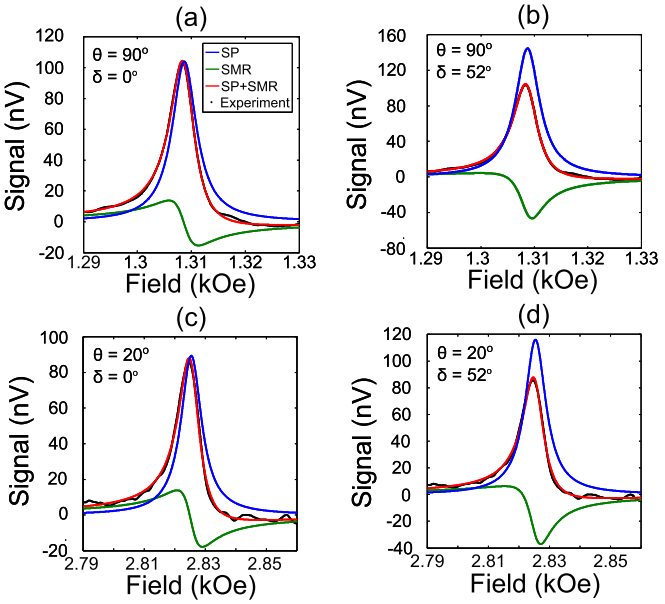

FIG. 4. (Color online) Representative fits of the ST-FMR data for both zero and nonzero values of δ. Additionally, we show fits to the data for two different angles, $\theta = 90^\circ$ and $\theta = 20^\circ$. These two angles each represent data acquired from regions **I** and **II** in Fig. 2. The black data points are densely packed together. The total theoretical fit is plotted in red, while the two contributions to the total, spin pumping and SMR, are plotted in blue and green, respectively.

composition begins to fluctuate. This region is indicated with a **I** and is shaded blue in Fig. 2. As seen in Fig. 2(b), for the smallest values of θ, $G^{\uparrow\downarrow}$ settles on having real and imaginary components with similar magnitude.

Previously reported experiments, where the applied magnetic field is in plane, report that $G^{\uparrow\downarrow}$ is mainly real, which is not consistent with our analysis so far. A possible explanation may involve the parameter δ. In fact, δ has been used in a similar ST-FMR experiment where the in-plane field configuration and a near out-of-plane measurement was performed while $G^{\uparrow\downarrow}$ was assumed to be real [44]. If we allow δ to vary, we find that for a value of $\delta = -52^\circ$ we had a local maximum in the ratio of $\mathrm{Re}(G^{\uparrow\downarrow})/|G^{\uparrow\downarrow}|$, at $\theta = 90^\circ$, as a function of δ. With this new value of δ, and with the same value of J_c and Θ_{SH} as before, we performed again the θ dependent analysis. The dependence that the magnitude of $G^{\uparrow\downarrow}$ has on θ with this nonzero δ is shown in Fig. 3(a) and is plotted as orange squares. Figure 2(c) shows the complex composition of $G^{\uparrow\downarrow}$ for this nonzero δ. In contrast to before, for region **II**, $G^{\uparrow\downarrow}$ is mostly real with little fluctuation in the angular range $\theta = 35^\circ$– 90°. However, this behavior does not persist; again we see that in region **I**, where the field approaches an OOP configuration, both the real and imaginary parts of $G^{\uparrow\downarrow}$ become appreciably nonzero. To illustrate how both assumptions that $\delta = 0^\circ$ and $\delta = -52^\circ$ both adequately fit the data, we plot the data with fits for both cases at $\theta = 90^\circ$ and $\theta = 20^\circ$ in Fig. 4.

2. *Analysis with correction for possible spin Seebeck contribution*

The fluctuating complex composition of $G^{\uparrow\downarrow}$ in the blue shaded regions of Fig. 3 is surprising and may indicate a problem with the model. This leads to our second approach

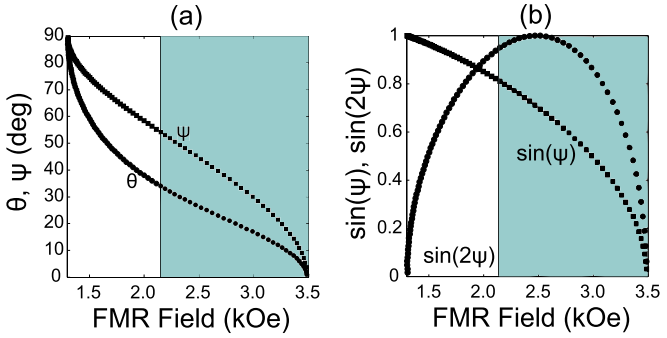

FIG. 5. (Color online) The θ and ψ dependence of the OOP polar angles are plotted in (a) as a function of the FMR field. In (b), we plot $\sin\psi$ and $\sin 2\psi$ as a function of the same FMR field. In blue we shade the region of FMR field space where our OOP analysis began to show strong angular dependence in the spin mixing conductance parameters. This region appears correlated with where $\sin\psi$ and $\sin 2\psi$ are comparable in magnitude.

of treating the data by subtracting an excessive symmetric portion of the line shape. We assume that the excessive symmetric signal has a $\sin\phi\sin\psi$ dependence. At $\phi = 45^\circ$ and $\psi = 90^\circ$ the contribution from this term can be obtained from the fit shown in Fig. 2 and it is roughly 30% of the total symmetric signal. Thus, by rotating OOP, the excessive contribution diminishes. At this point there is a attractive qualitative argument that suggests this approach has merit. In Fig. 5(a) the position of θ and ψ at the FMR resonance field is plotted by simultaneously solving Eqs. (5) and (6). The blue shaded region is the angular range where the $G^{\uparrow\downarrow}$ fit parameters in Fig. 3 began to fluctuate. In Fig. 5(b) the value of $\sin 2\psi$ and $\sin\psi$ is plotted as a function of the FMR field with the same shaded region as in Fig. 5(a). The reason $\sin 2\psi$ is shown is because Eqs. (6) and (7) have nonzero terms proportional to $\sin 2\psi$ and $\cos\psi\sin 2\psi$ for $\psi < 90^\circ$. If the "excess" spin pumping term has the angular dependence $\sin\phi\sin\psi$, it will be put in contention with the model where the values of terms proportional to $\sin 2\psi$ becomes appreciable. The blue shaded region in Fig. 5(b) corresponds to the angular range in Fig. 3 where $G^{\uparrow\downarrow}$ fluctuates, and it is near where $\sin 2\psi$ and $\sin\psi$ are of equal magnitude.

In Figs. 6(a) and 6(b), the original trace and a 32.5% reduced symmetric amplitude trace at $\phi = 45^\circ$ and $\psi = 90^\circ$ are shown with respective fits to the SMR/SP model. Here, we have gone back to our original assumption that $\delta = 0^\circ$, while keeping $J_c = 9 \times 10^8$ A/m^2 and $\Theta_{\mathrm{SH}} = 0.09$. The free parameters in the fit are as before: the magnitude of $G^{\uparrow\downarrow}$, and the real and imaginary parts of $G^{\uparrow\downarrow}$. Flexibility in the model still allows both traces to be fit well, but the values of the fit parameters shift. As can be expected from the reduced signal, the magnitude of the spin mixing conductance is lowered. The more interesting change in the fit parameters is illustrated in Fig. 6(c). In Fig. 6(c), the x axis is a percentage of the symmetric signal that is removed from the raw data, the orange squares correspond to the ratio of $\mathrm{Im}(G^{\uparrow\downarrow})/|G^{\uparrow\downarrow}|$, and the black circles are a ratio of $\mathrm{Re}(G^{\uparrow\downarrow})/|G^{\uparrow\downarrow}|$. As the percentage of the subtracted symmetric signal is increased, $\mathrm{Re}(G^{\uparrow\downarrow})$ grows while $\mathrm{Im}(G^{\uparrow\downarrow})$ decreases. When the subtracted percentage is greater than 32.5%, no further changes appear

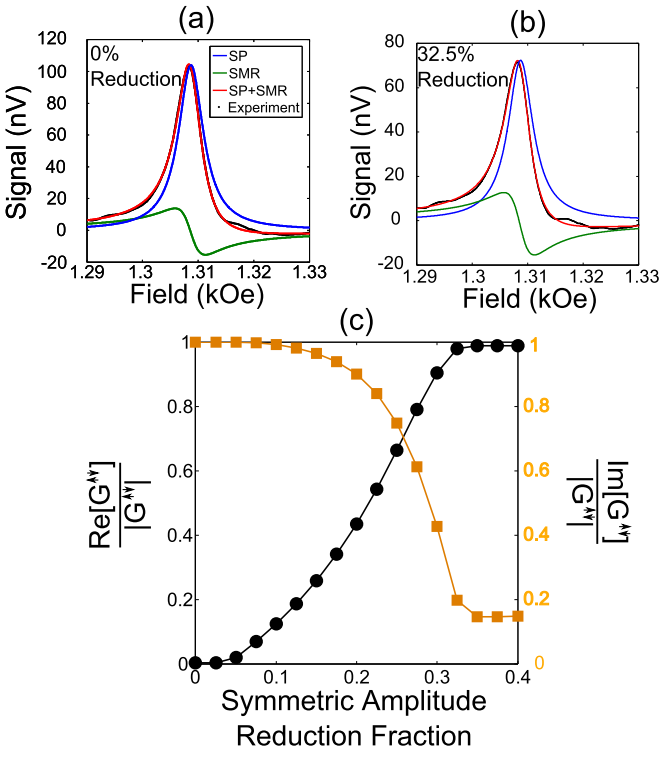

FIG. 6. (Color online) In (a) and (b), an original and an artificial, symmetric amplitude reduced ST-FMR signal is shown for the orientation $\phi = 45°$ and $\theta = 90°$. The model is able to fit both traces, but to do so the relative proportions of the real and imaginary part of $G^{\uparrow\downarrow}$ have shifted. To illustrate this, in (c) we plot the ratio of the real part of $G^{\uparrow\downarrow}$ to the magnitude of $G^{\uparrow\downarrow}$ as black circles as a function of a percentage of the symmetric signal that is artificially removed. Orange circles are the ratio of the imaginary part of $G^{\uparrow\downarrow}$ to the magnitude of $G^{\uparrow\downarrow}$. Near a 30% reduction of the symmetric signal, both curves seem to saturate.

and $G^{\uparrow\downarrow}$ is mostly real. This may be indirect evidence that the model may be correct for $\delta = 0°$ if the correction through subtraction of the symmetric signal is made.

To test the proposed $\sin\phi \sin\psi$ angular dependence of the additional spin pumping term, a symmetric signal was subtracted from the OOP angular data set shown in Fig. 1. For $\psi = 90°$, the percentage that was initially subtracted was the 32.5% value obtained from Fig. 2. The results are shown in Fig. 7 and should be compared to those shown in Fig. 3. While $G^{\uparrow\downarrow}$ stays mostly real for near in-plane angles as θ decreases below 70°, fluctuations in the complex composition of $G^{\uparrow\downarrow}$ again occur. Thus, it appears that although the correction we employed allows for a mostly real $G^{\uparrow\downarrow}$ with $\delta = 0°$ for small tipping angles, it actually predicts even larger fluctuations in the θ dependence of $G^{\uparrow\downarrow}$.

Before concluding, it is important to step back and summarize the results of the in-plane analysis and the implications it had on an OOP analysis. The ϕ dependence of the symmetric part of the ST-FMR line shape is predicted to have a $\sin 2\phi \cos\phi$ angular dependence. Although the dominant contribution to the ϕ dependence was of this form, an unexpected $\sin\phi$ dependence was observed. With this in mind, when analyzing the OOP data we tried two different

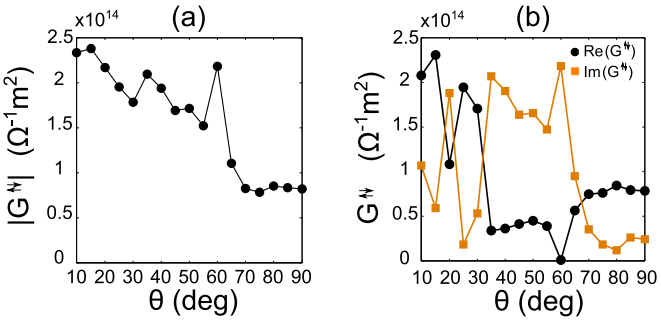

FIG. 7. (Color online) Plot of the magnitude of $G^{\uparrow\downarrow}$ in (a) and the complex component of $G^{\uparrow\downarrow}$ in (b) for our line-shape corrected analysis as a function of θ. This analysis should be compared to that shown in Fig. 3 for the uncorrected data.

methods. The first method was agnostic towards this additional $\sin\phi$ dependence. We found that for $\delta = 0°$, $G^{\uparrow\downarrow}$ started off as being purely imaginary for $\theta = 90°$. As the field was tipped, the complex composition of $G^{\uparrow\downarrow}$ began to fluctuate and both a sizable real and imaginary component of $G^{\uparrow\downarrow}$ was required. By setting $\delta = -52°$, $G^{\uparrow\downarrow}$ became mostly real at $\theta = 90°$. However, again as we tipped OOP, there was fluctuation in $G^{\uparrow\downarrow}$. The second method attempted to subtract out "excess" symmetric signal from the line shape as a correction. The assumed angular dependence of this excess signal was $\sin\psi \sin\phi$. The corrected analysis on the in-plane ST-FMR data predicted a mostly real $G^{\uparrow\downarrow}$ for $\delta = 0°$. This result seemed satisfying as a mostly real $G^{\uparrow\downarrow}$ was obtained without the invocation of another fit parameter (δ). However, the OOP analysis began to show fluctuations in the complex composition of $G^{\uparrow\downarrow}$ at even smaller tipping angles. Irrespective of whether or not a "correction" took place, the OOP angular analysis always extracts changes in the complex composition of $G^{\uparrow\downarrow}$ for arbitrary OOP angles. On a phenomenological level this can be interpreted as a change in the fraction of spin transfer torque from the SHE behaving as a fieldlike torque compared to the fraction acting as a dampinglike torque.

Another possibility is that the assumption of a fixed δ for arbitrary OOP field directions may not be valid. One reason could be a variation of the inductively coupled rf current from the oscillating ferromagnetic magnetization [45]. Further studies with different field directions and layer thicknesses of both Pt and YIG may help to resolve these issues. Finally, we note that we do not have the experimental capability to conduct a ϕ dependent study at an arbitrary θ. Such a capability could prove invaluable in unraveling the origin of the additional ϕ dependence that was observed, as well as providing more data to better constrain a model with a large number of parameters.

IV. CONCLUSIONS

The ST-FMR paradigm has been studied with great intensity for spin Hall metal/ferromagnet bilayers where the ferromagnet is a conductor. The present work shows that it can be successfully extended to insulating FM materials. Furthermore, it is clear that, in addition to an Oersted microwave field torque from the Pt strip line, an additional spin torque from spin accumulation at the Pt/YIG drives the dynamics as well.

This particular conclusion is bolstered by a good agreement with theory that includes such spin torques. A very interesting property of bilayers with ferromagnetic insulators such as YIG is that the longitudinal voltage generated along the Pt when ST-FMR is taking place is created by effects that all trace their origin back to the SHE. These detection mechanisms set this work apart from metallic ferromagnets, where mixing of the microwave current with the AMR of the ferromagnet itself leads to a measurable voltage. In this work we have also tested a recently proposed model [36] that describes ST-FMR voltages in YIG/Pt bilayers. In employing this model, under various assumptions and potential corrections, we found that in order to adequately fit our data over the full OOP angle range, the complex composition of $G^{\uparrow\downarrow}$ had OOP angular dependence. This may indicate that further refinement of the theory may be required to account for additional resonant contributions, e.g., from the spin Seebeck effect.

ACKNOWLEDGMENTS

We acknowledge Stephen Wu for assistance with ion milling used for sample preparation. The work at Argonne was supported by the U.S. Department of Energy, Office of Science, Materials Science and Engineering Division. Lithography was carried out at the Center for Nanoscale Materials, which is supported by DOE, Office of Science, Basic Energy Science under Contract No. DE-AC02-06CH11357. Work at Northwestern utilized facilities maintained by the NSF supported Northwestern Materials Research Center under Contract No. DMR-1121262. The work at Colorado State University was supported by the U. S. Army Research Office (W911NF-14-1-0501), the U. S. National Science Foundation (ECCS-1231598), C-SPIN (one of the SRC STARnet Centers sponsored by MARCO and DARPA), and the U. S. Department of Energy (DE-SC0012670).

[1] *Recent Advances in Magnetic Insulators—From Spintronics to Microwave Applications*, edited by M. Wu and A. Hoffmann, Solid State Physics Vol. 64 (Academic, New York, 2013).
[2] H. L. Wang, C. H. Du, P. C. Hammel, and F. Y. Yang, Phys. Rev. B **89**, 134404 (2014).
[3] H. Chang, P. Li, W. Zhang, T. Liu, A. Hoffmann, L. Deng, and M. Wu, IEEE Magn. Lett. **5**, 6700104 (2014).
[4] P. Pirro, T. Brächer, A. V. Chumak, B. Lägel, C. Dubs, O. Surzhenko, P. Görnert, B. Leven, and B. Hillebrands, Appl. Phys. Lett. **104**, 012402 (2014).
[5] A. Hoffmann and H. Schultheiß, Curr. Opin. Solid State Mat. Sci. **19**, 253 (2015).
[6] Y. Kajiwara, K. Harii, S. Takahashi1, J. Ohe, K. Uchida, M. Mizuguchi, H. Umezawa, H. Kawai, K. Ando, K. Takanashi, S. Maekawa1, and E. Saitoh, Nature (London) **464**, 262 (2010).
[7] A. Hamadeh, O. d'Allivy Kelly, C. Hahn, H. Meley, R. Bernard, A. H. Molpeceres, V. V. Naletov, M. Viret, A. Anane, V. Cros, S. O. Demokritov, J. L. Prieto, M. Muñoz, G. de Loubens, and O. Klein, Phys. Rev. Lett. **113**, 197203 (2014).
[8] M. I. Dyakonov and V. I. Perel, Sov. Phys. JETP **13**, 467 (1971).
[9] J. E. Hirsch, Phys. Rev. Lett. **83**, 1834 (1999).
[10] A. Hoffmann, IEEE Trans. Magn. **49**, 5172 (2013).
[11] W. Zhang, M. B. Jungfleisch, W. Jiang, J. Sklenar, F. Y. Fradin, J. E. Pearson, J. B. Ketterson, and A. Hoffmann, J. Appl. Phys. **117**, 172610 (2015).
[12] L. Liu, T. Moriyama, D. C. Ralph, and R. A. Buhrman, Phys. Rev. Lett. **106**, 036601 (2011).
[13] A. R. Mellnik, J. S. Lee, A. Richardella, J. L. Grab, P. J. Mintun, M. H. Fischer, A. Vaezi, A. Manchon, E.-A. Kim, N. Samarth, and D. C. Ralph, Nature (London) **511**, 449 (2014).
[14] J. C. Sankey, P. M. Braganca, A. G. F. Garcia, I. N. Krivorotov, R. A. Buhrman, and D. C. Ralph, Phys. Rev. Lett. **96**, 227601 (2006).
[15] H. J. Juretschke, J. Appl. Phys. **31**, 1401 (1960).
[16] M. I. Dyakonov, Phys. Rev. Lett. **99**, 126601 (2007).
[17] Y. S. Gui, N. Mecking, X. Zhou, G. Williams, and C.-M. Hu, Phys. Rev. Lett. **98**, 107602 (2007).
[18] H. Nakayama, M. Althammer, Y.-T. Chen, K. Uchida, Y. Kajiwara, D. Kikuchi, T. Ohtani, S. Geprägs, M. Opel, S. Takahashi, R. Gross, G. E. W. Bauer, S. T. B. Goennenwein, and E. Saitoh, Phys. Rev. Lett. **110**, 206601 (2013).
[19] Y.-T. Chen, S. Takahashi, H. Nakayama, M. Althammer, S. T. B. Goennenwein, E. Saitoh, and G. E. W. Bauer, Phys. Rev. B **87**, 144411 (2013).
[20] M. Althammer *et al.*, Phys. Rev. B **87**, 224401 (2013).
[21] C. Hahn, G. de Loubens, O. Klein, M. Viret, V. V. Naletov, and J. Ben Youssef, Phys. Rev. B **87**, 174417 (2013).
[22] J. C. Rojas-Sanchez, N. Reyren, P. Laczkowski, W. Savero, J.-P. Attane, C. Deranlot, M. Jamet, J.-M. George, L. Vila, and H. Jaffres, Phys Rev. Lett. **112**, 106602 (2014).
[23] W. Zhang, M. B. Jungfleisch, W. Jiang, J. E. Pearson, A. Hoffmann, F. Freimuth, and Y. Mokrousov, Phys. Rev. Lett. **113**, 196602 (2014).
[24] W. Zhang, M. B. Jungfleisch, F. Freimuth, W. Jiang, J. Sklenar, J. E Pearson, J. B. Ketterson, Y. Mokrousov, and A. Hoffmann, Phys. Rev. B **92**, 144405 (2015).
[25] B. F. Miao, S. Y. Huang, D. Qu, and C. L. Chien, Phys. Rev. Lett. **112**, 236601 (2014).
[26] V. L. Grigoryan, W. Guo, G. E. W. Bauer, and J. Xiao, Phys. Rev. B **90**, 161412 (2014).
[27] W. Zhang, M. B. Jungfleisch, W. Jiang, J. E. Pearson, and A. Hoffmann, J. Appl. Phys. **117**, 17C727 (2015).
[28] H. Jiao and G. E. W. Bauer, Phys. Rev. Lett. **110**, 217602 (2013).
[29] W. Zhang, M. B. Jungfleisch, W. Jiang, Y. Liu, J. E. Pearson, S. G. E. te Velthuis, A. Hoffmann, F. Freimuth, and Y. Mokrousov, Phys. Rev. B **91**, 115316 (2015).
[30] Y. Tserkovnyak, A. Brataas, and G. E. W. Bauer, Phys. Rev. Lett. **88**, 117601 (2002).
[31] M. Weiler, M. Althammer, M. Schreier, J. Lotze, M. Pernpeintner, S. Meyer, H. Huebl, R. Gross, A. Kamra, J. Xiao, Y. T. Chen, H. J. Jiao, G. E. W. Bauer, and S. T. B. Goennenwein, Phys. Rev. Lett. **111**, 176601 (2013).
[32] O. Mosendz, V. Vlaminck, J. E. Pearson, F. Y. Fradin, G. E. W. Bauer, S. D. Bader, and A. Hoffmann, Phys. Rev. B **82**, 214403 (2010).
[33] L. Bai, P. Hyde, Y. S. Gui, C.-M. Hu, V. Vlaminck, J. E. Pearson, S. D. Bader, and A. Hoffmann, Phys. Rev. Lett. **111**, 217602 (2013).

[34] T. Kikkawa, K. Uchida, Y. Shiomi, Z. Qiu, D. Hou, D. Tian, H. Nakayama, X.-F. Jin, and E. Saitoh, Phys. Rev. Lett. **110**, 067207 (2013).
[35] M. B. Jungfleisch, V. Lauer, R. Neb, A. V. Chumak, and B. Hillebrands, Appl. Phys. Lett. **103**, 022411 (2013).
[36] T. Chiba, M. Schreier, G. E. W. Bauer, and S. Takahashi, J. Appl. Phys. **117**, 17C715 (2015).
[37] N. Vlietstra, J. Shan, V. Castel, J. Ben Youssef, G. E. W. Bauer, and B. J. van Wees, Appl. Phys. Lett. **103**, 032401 (2013).
[38] S. Meyer, R. Schlitz, S. Geprägs, M. Opel, H. Huebl, R. Gross, and S. T. B. Goennenwein, Appl. Phys. Lett. **106**, 132402 (2015).
[39] T. Liu, H. Chang, V. Vlaminck, Y. Sun, M. Kabatek, A. Hoffmann, L. Deng, and M. Wu, J. Appl. Phys. **115**, 17A501 (2014).
[40] M. B. Jungfleisch, W. Zhang, W. Jiang, H. Chang, J. Sklenar, S. M. Wu, J. E. Pearson, A. Bhattacharya, J. B. Ketterson, M. Wu, and A. Hoffmann, J. Appl. Phys. **117**, 17D128 (2015).
[41] T. Skinner, Ph.D. dissertation, University of Cambridge, 2014.
[42] T. Chiba, G. E. W. Bauer, and S. Takahashi, Phys. Rev. Appl. **2**, 034003 (2014).
[43] W. Zhang, V. Vlaminck, J. E. Pearson, R. Divan, S. D. Bader, and A. Hoffmann, Appl. Phys. Lett. **103**, 242414 (2013).
[44] M. Schreier, T. Chiba, A. Niedermayr, J. Lotze, H. Huebl, S. Geprägs, S. Takahashi, G. E. W. Bauer, R. Gross, and S. T. B. Goennenwein, Phys. Rev. B **92**, 144411 (2015).
[45] M. Weiler, J. M. Shaw, H. T. Nembach, and T. J. Silva, Phys. Rev. Lett. **113**, 157204 (2014).